Available online at www.sciencedirect.com
ScienceDirect
Journal of Sound and Vibration 302 (2007) 728–745
JOURNAL OF SOUND AND VIBRATION
www.elsevier.com/locate/jsvi

Modelling of wave propagation in composite plates using the time domain spectral element method

Paweł Kudela[a], Arkadiusz Żak[a], Marek Krawczuk[a,b], Wiesław Ostachowicz[a,c,*]

[a]*Institute of Fluid Flow Machinery, Polish Academy of Sciences, Gdansk, Poland*
[b]*Faculty of Electrical and Control Engineering, Gdansk University of Technology, Poland*
[c]*Faculty of Navigation, Gdynia Maritime University, Poland*

Received 17 May 2006; received in revised form 1 December 2006; accepted 4 December 2006
Available online 12 February 2007

Abstract

This paper presents results of numerical simulation of the propagation of transverse elastic waves corresponding to the A0 mode of Lamb waves in a composite plate. The problem is solved by the Spectral Element Method. Spectral plate finite elements with 36 nodes defined at Gauss–Lobatto–Legendre points are used. As a consequence of the selection of Lagrange polynomials for element shape functions discrete orthogonality is obtained leading to the diagonal form of the element mass matrix. This results in a crucial reduction of numerical operations required for the solution of the equation of motion by time integration. Numerical calculations have been carried out for various orientations and relative volume fractions of reinforcing fibres within the plate. The paper shows how the velocities of transverse elastic waves in composite materials depend on the orientation and the relative volume fraction of the reinforcement.

1. Introduction

Composite materials are ideal for structural applications where high strength-to-weight and stiffness-to-weight ratios are required. Aircraft and spacecraft are typical weight-sensitive structures in which composite materials are cost-effective so that their use has substantially increased over past decades. Composite materials possess unique advantages over their metallic counterparts, but they also present researchers and designers with complex and challenging problems [1–6].

Damage initiation and growth in structural elements is a very significant problem since in most cases it leads to catastrophic accidents. In the case of structural elements made out of composite materials, delamination, fibre breaking, and matrix cracking are especially dangerous failure modes. This is why, in order to improve the safety and reliability of such structures, periodic inspections are necessary. For this reason a variety of on-line structural health monitoring (SHM) systems and strategies have been developed and used based on piezoelectric sensors and elastic wave propagation.

*Corresponding author. Institute of Fluid Flow Machinery, Polish Academy of Sciences, Gdansk, Poland.
E-mail address: wieslaw@imp.gda.pl (W. Ostachowicz).

0022-460X/$ - see front matter © 2007 Elsevier Ltd. All rights reserved.
doi:10.1016/j.jsv.2006.12.016

Impact wave signals are generated by piezoelectric actuators and usually these are various modes of Lamb waves. Next, waves propagate and system response is registered in piezoelectric sensors embedded in a structure. The signals registered are used as input for further processing with damage detection algorithm. In practical applications, due to a simpler interpretation of measured responses, signals which correspond to the fundamental modes of Lamb waves are considered, these being A0 and S0 modes. Furthermore, the A0 mode excited in composite materials is characterised by a much stronger out-of-plane motion than the S0 mode. This makes the A0 mode more suitable for measurements in the case of plate-like structures and for that reason the modelling of the A0 mode in the present analysis seems sufficient and justified.

The main problems in the analysis of high frequency (50–350 kHz) elastic waves propagating at velocities about 1 km/s in composite elements of structures are related to spatial discretisation. In order to obtain an accurate solution of the equation of motion and to capture the effect of wave scattering at boundaries and structural discontinuities a huge number of degrees of freedom (dof) is necessary. Conventional modal methods, when extended to high frequency regimes, become computationally inefficient since many higher modes that should participate in motion are misrepresented. For a specific geometry and finite periodic or semi-infinite boundary conditions many different solution techniques have been proposed and reported so far—an excellent overview of theses techniques is given in Ref. [7].

Among many methods used for modelling and studying the phenomena of propagation of elastic waves such numerical methods can be marked as: the finite difference method (FDM) [8], the finite element method (FEM) [9–14], the boundary element method (BEM) [15,16]. However, they are not only time consuming, but also require large computational memory in the case of simple two-dimensional (2D) wave propagation problems. On the other hand, the finite strip element method (FSEM) and semi-numerical method (SNM) [17–19] require much less memory storage space for necessary data due to a lower level of discretisation and application of the exact solution in one direction. SNM is very effective for the computation of forced wave motion in the frequency domain and can be used for much higher frequencies than the methods based on FEM. As with BEM, FSEM uses Green's function but in a different manner. On the other hand, variable size of strip stiffness matrix and modification of spline functions at boundary nodes are inconvenient features of the method.

A method that incorporates the advantages of FEM (discretisation) and the FDM (time integration schemes) is the unstructured grid method (UGM) [20,21]. This method is based on the dynamic equilibrium equations of computational cells formed around auxiliary triangular grids. The solution is obtained by the alternative calculation of nodal displacements and central point stresses of spatial grids.

A different approach has been proposed in Refs. [22,23]. In the mass-spring-lattice-model (MSLM) inertia and stiffness properties are calculated using lumped parameters. Recent developments in this area include a new local interaction simulation approach (LISA) [24–26]. This method does not use a finite difference equation, but simulates wave propagation heuristically, i.e. directly from physical phenomena and properties.

More recently various spectral methods have been proposed for the analysis of elastic wave propagation in complex media [27,28]. It should be stressed that, despite the terminology, these methods are completely different.

The fast Fourier transformation (FFT)-based spectral element method (SEM) proposed by Doyle [27] is very similar to the technique of the FEM as far as the assembly and the solution of the equation of motion is concerned. The formulation of this method starts from exact solutions of the governing partial differential equations in the frequency domain. Excitation signals are transformed into a number of frequency components using FFT. Next as a part of a big frequency loop the dynamic stiffness matrix is generated, transformed, and solution is found for each unit impulse at each frequency. This yields directly to frequency response function (FRF) of an analysed problem. The calculated frequency domain responses are then transformed back to the time domain using inverse fast Fourier transformation (IFFT). This technique is well suited to simple 1D problems [29–31], but becomes difficult to use for complex geometries (additional throw-off elements are demanded). Some difficulties also arise with the periodic nature of FFT when 2D or 3D problems must be analysed. However, recent work in this area shows the application of the FFT-based SEM to wave propagation phenomena in anisotropic plates and inhomogeneous layered media [32–34].

The SEM as proposed by Patera in 1984 [28] is much more versatile for the investigation of the propagation of elastic waves in structures of complex geometries. This method originates from the use of spectral series for

the solution of partial differential equations [35]. The idea of SEM is very similar to FEM except for the specific approximation functions it uses. Elemental interpolation nodes are located at points corresponding to zeros of an appropriate family of orthogonal polynomials (Legendre or Chebyshev). A set of local s hape functions consisting of Lagrange polynomials, which are spanned on these points, are built and used. As a consequence of this, as well as the use of the Gauss-Lobatto-Legendre integration rule, a diagonal form of the mass matrix is obtained. In this way the cost of numerical calculations is much less expensive than in the case of any classic FE approach. Moreover, the numerical errors decrease faster than any power of $1/p$ (so-called 'spectral convergence'), where p is the order of the applied polynomial [36]. The main fields of application of SEM nowadays include: fluid dynamics [37], heat transfer [38], acoustics [39], seismology [40], etc.

However, it appears that the use of SEM for problems of propagation of elastic waves in 2D structural elements made out of composite materials has not been widely reported in the literature so far. The use of the SEM for wave propagation in anisotropic crystals only has been considered [41] and the application of the SEM to wave propagation in anisotropic and inhomogeneous uncracked and cracked beams [42]. The method presented can be considered as an alternative to the FFT-based SEM. The aim of this paper is to develop a spectral plate finite element, which next can be successfully used for the analysis of the propagation of transverse (out-off-plane or flexural) elastic waves in a composite plate. In order to model A0 Lamb mode accurately the first-order shear deformation theory for plates is applied. Numerical calculations presented in this work have been carried out for various orientations and relative volume fractions of reinforcing fibres. The following study of simulated wave propagation in composite plates provides useful information which can be used in SHM system design.

2. Spectral plate finite element formulation

2.1. Definition of element nodes

Nodes of a spectral plate finite element are defined in the local coordinate system of the element $\xi\eta$ as roots of the following polynomial expression:

$$\begin{cases} (1-\xi^2)P'_N(\xi) = 0, \\ (1-\eta^2)P'_N(\eta) = 0, \end{cases} \tag{1}$$

where $\xi,\eta \in [-1,1]$ and where P_N is the Nth order Legendre polynomial. The symbol $'$ denotes the first derivative. In this way the nodes of the element can be specified in the local coordinate system of the element. In the current formulation the fifth-order Legendre polynomial is chosen, hence 36 nodes can be specified in

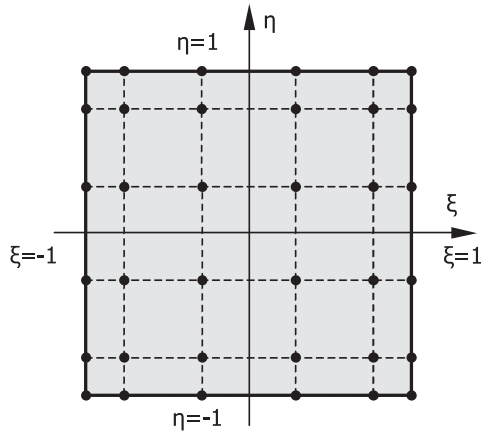

Fig. 1. A 36-node spectral finite element in the local coordinate.

the local coordinate system of the element $\xi\eta$ as (see Fig. 1 for details):

$$(\xi_m, \eta_n) \quad m, n = 1, 2, \ldots, 6,$$
$$\xi_m, \eta_n \in \left\{ -1, -\sqrt{\frac{1}{3}+\frac{2}{3\sqrt{7}}}, -\sqrt{\frac{1}{3}-\frac{2}{3\sqrt{7}}}, \sqrt{\frac{1}{3}-\frac{2}{3\sqrt{7}}}, \sqrt{\frac{1}{3}+\frac{2}{3\sqrt{7}}}, 1 \right\}. \tag{2}$$

It can be seen from Fig. 1 that the present definition of the element nodes results in a irregular distribution of the nodes within the element contrary to the classical FE approach, when the element nodes are uniformly spaced within elements.

2.2. Element shape functions

A set of shape functions can be built on the specified nodes to approximate the geometry of the element in the global coordinate system xy and also to approximate the transverse w and the angular α, β, displacements within the element. The same shape functions are used for both coordinates x and y as well as for all displacement components.

The Lagrange interpolation function supported on the element nodes can be written as follows:

$$\begin{cases} x(\xi,\eta) = \sum_{k=1}^{36} N_k^*(\xi,\eta) x_k = \sum_{m=1}^{6}\sum_{n=1}^{6} N_m(\xi) N_n(\eta) x_{mn}, \\ y(\xi,\eta) = \sum_{k=1}^{36} N_k^*(\xi,\eta) y_k = \sum_{m=1}^{6}\sum_{n=1}^{6} N_m(\xi) N_n(\eta) y_{mn}, \end{cases} \tag{3a}$$

$$\begin{cases} \bar{w}(\xi,\eta) = \sum_{k=1}^{36} N_k^*(\xi,\eta) \bar{w}_k = \sum_{m=1}^{6}\sum_{n=1}^{6} N_m(\xi) N_n(\eta) \bar{w}_{mn}, \\ \bar{\alpha}(\xi,\eta) = \sum_{k=1}^{36} N_k^*(\xi,\eta) \bar{\alpha}_k = \sum_{m=1}^{6}\sum_{n=1}^{6} N_m(\xi) N_n(\eta) \bar{\alpha}_{mn}, \\ \bar{\beta}(\xi,\eta) = \sum_{k=1}^{36} N_k^*(\xi,\eta) \bar{\beta}_k = \sum_{m=1}^{6}\sum_{n=1}^{6} N_m(\xi) N_n(\eta) \beta\bar{\beta}_{mn}, \end{cases} \tag{3b}$$

where $N_m(\xi)$ and $N_n(\eta)$ are 1D shape functions of the element (in the local coordinate system of the element $\xi\eta$) while x_k and y_k, denote the coordinates x and y of the element nodes. Nodal values of the transverse and angular displacements are denoted as $\bar{w}$, $\bar{\alpha}$, $\bar{\beta}$, respectively. Positive values of the nodal displacements are shown in Fig. 2.

It should be mentioned here that the approximation shape functions $N_m(\xi)$ and $N_n(\eta)$ are orthogonal in a discrete sense:

$$\int_{-1}^{1} N_m(\xi) N_n) \mathrm{d}\xi = \sum_{k=1}^{6} w_k N_m(\xi_k) N_n(\xi_k) = w_m \delta_{mn}, \quad m, n = 1, \ldots, 6, \tag{4}$$

where w_k is the Gauss–Lobatto weight defined later, δ_{mn} is the Kronecker delta. The shape functions for element nodes (i.e. 1, 11, 22, and 34) are presented in Fig. 3.

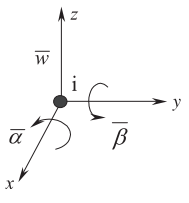

Fig. 2. Positive values of nodal degrees of freedom.

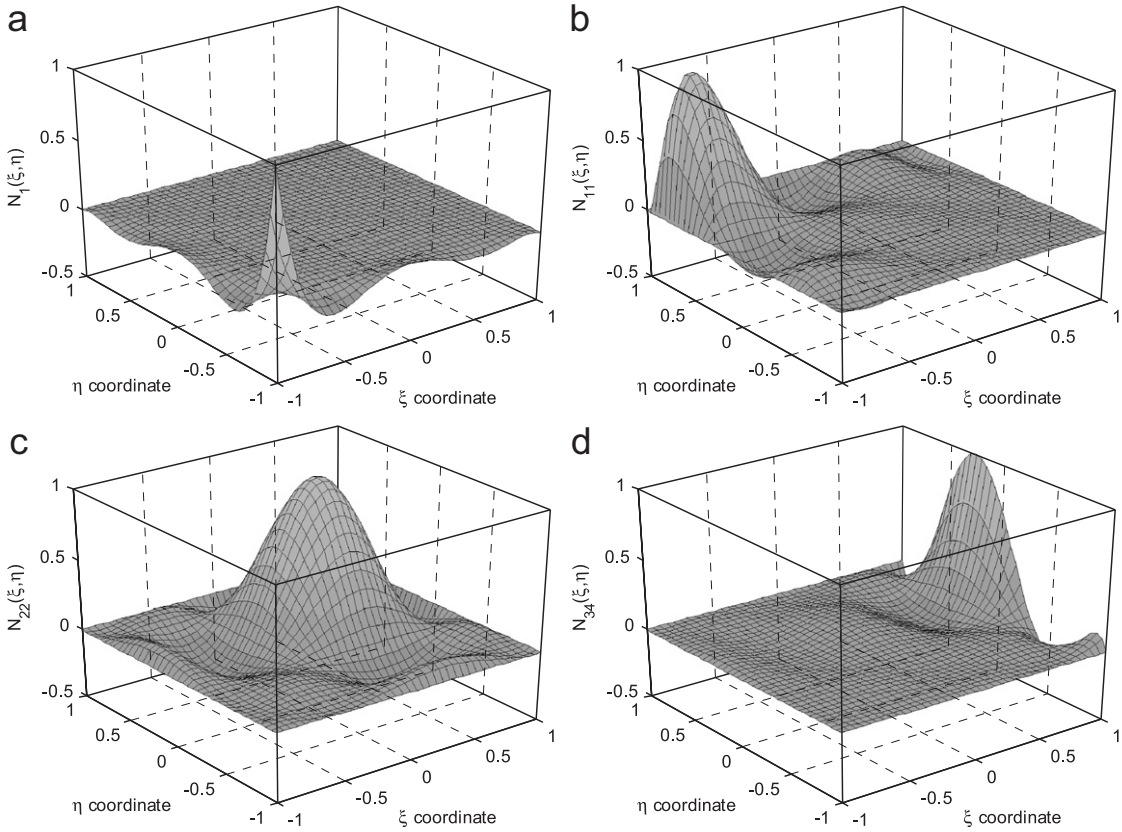

Fig. 3. Selected shape functions for a 36-node spectral plate finite.

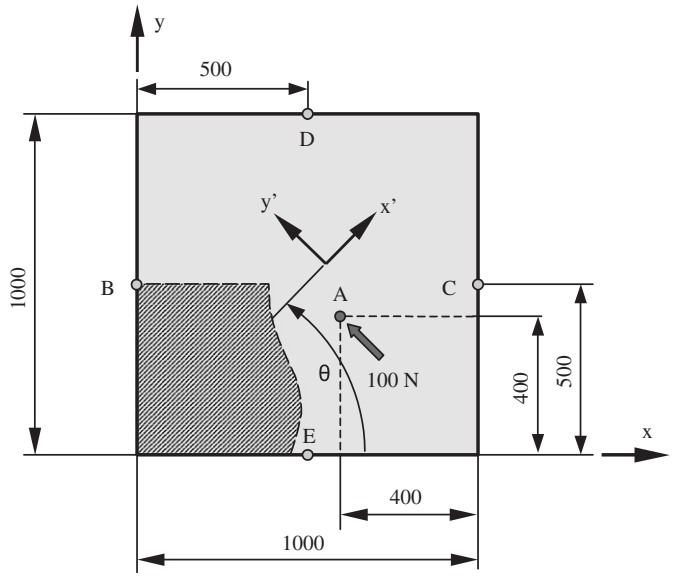

Fig. 4. A composite plate under investigation.

2.3. Mass and stiffness matrices

Based on Mindlin's theory for plates the displacement field within the element can be expressed as

$$\begin{cases} u(x,y,z) = z\,\bar{\alpha}(x,y), \\ v(x,y,z) = -z\,\bar{\beta}(x,y), \\ w(x,y,z) = \bar{w}(x,y). \end{cases} \tag{5a}$$

The independent rotations $\bar{\alpha}(x,y)$ and $\bar{\beta}(x,y)$ and transverse displacement $\bar{w}(x,y)$ are assumed in the following form (see also Eq. (3b)):

$$\begin{Bmatrix} \bar{w}(\xi,\eta) \\ \bar{\beta}(\xi,\eta) \\ \bar{\alpha}(\xi,\eta) \end{Bmatrix} = \mathbf{Nq} = \sum_{k=1}^{36} [N_k^*(\xi,\eta)] \begin{Bmatrix} \bar{w}_k \\ \bar{\beta}_k \\ \bar{\alpha}_k \end{Bmatrix}, \tag{5b}$$

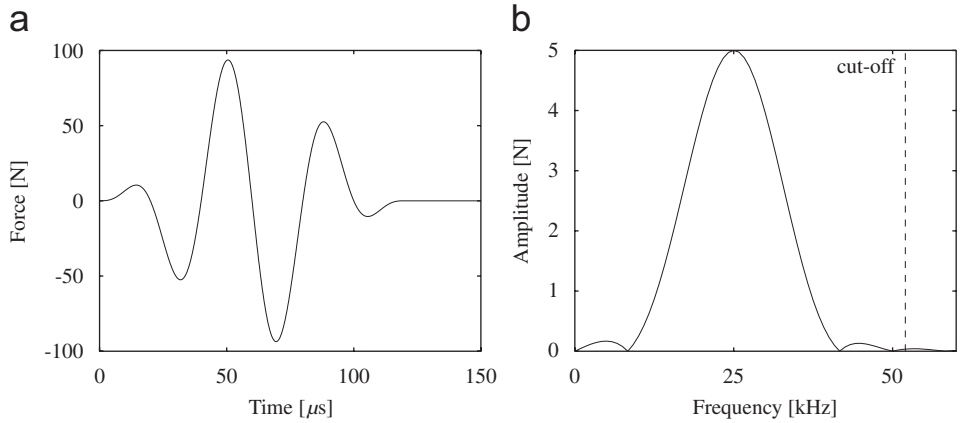

Fig. 5. An excitation signal in the form of a force pulse in (a) time, (b) frequency domain.

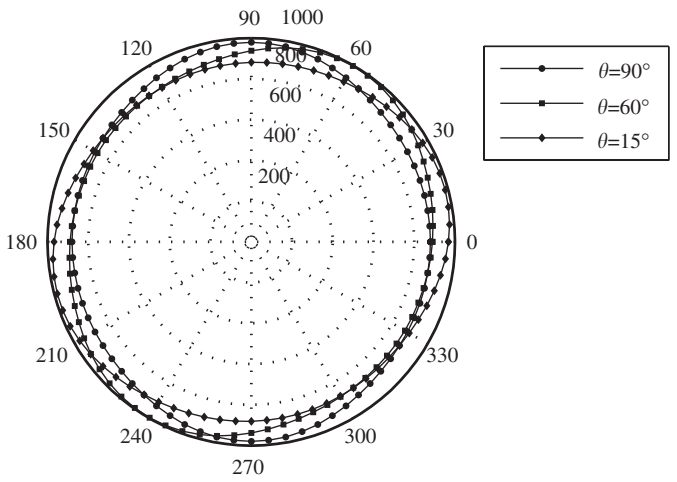

Fig. 6. Group velocity surfaces for a single layer of glass/epoxy laminate (vol = 25%).

where **N** denotes the shape function matrix and **q** is the vector of nodal variables. Based on the given displacement field the strains within the element can be expressed according to a standard FE formula as

$$\begin{Bmatrix} \varepsilon_{xx}(\xi,\eta) \\ \varepsilon_{yy}(\xi,\eta) \\ \gamma_{xy}(\xi,\eta) \\ \gamma_{xz}(\xi,\eta) \\ \gamma_{yz}(\xi,\eta) \end{Bmatrix} = \mathbf{Bq} = \sum_{k=1}^{36} [B_k(\xi,\eta)] \begin{Bmatrix} \bar{w}_k \\ \bar{\beta}_k \\ \bar{\alpha}_k \end{Bmatrix}, \tag{6}$$

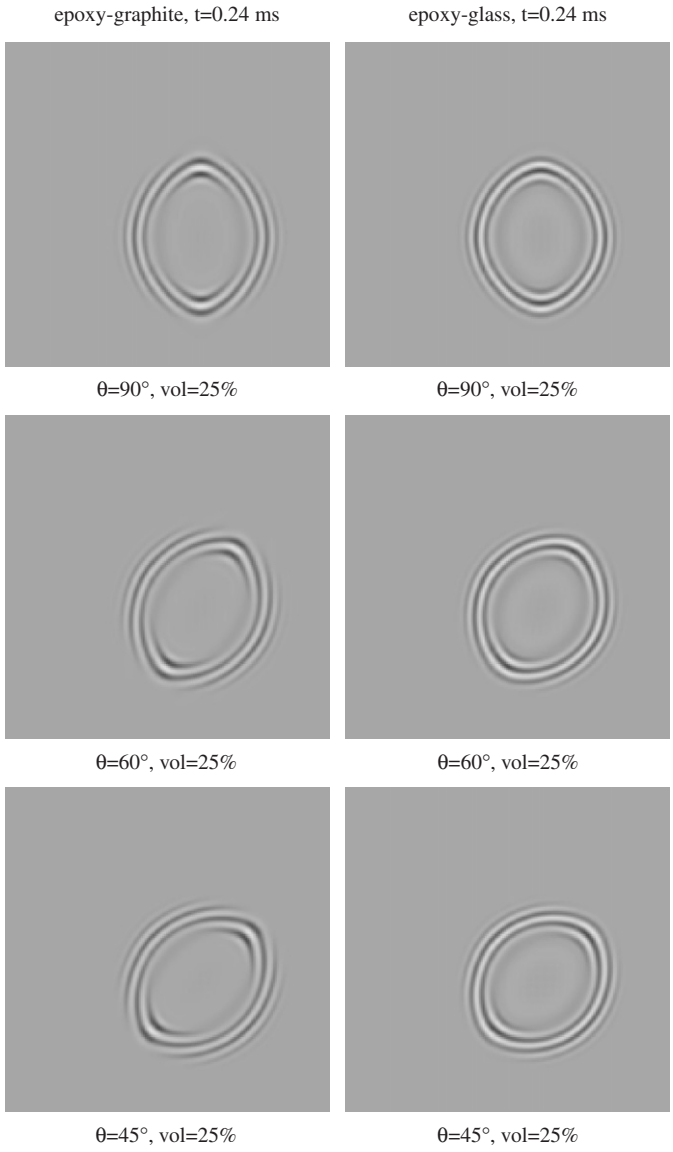

Fig. 7. Front of propagating transverse wave for a single layer.

where **B** is the strain–displacement matrix which can be calculated as

$$[B_k(\xi,\eta)] = \begin{bmatrix} 0 & 0 & \partial_x N_k^* \\ 0 & \partial_y N_k^* & 0 \\ 0 & -\partial_x N_k^* & \partial_y N_k^* \\ \partial_x N_k^* & 0 & N_k^* \\ \partial_y N_k^* & -N_k^* & 0 \end{bmatrix}, \quad \begin{Bmatrix} \partial_x N_k^* \\ \partial_y N_k^* \end{Bmatrix} = \mathbf{J}^{-1} \begin{Bmatrix} \partial_\xi N_k^* \\ \partial_\eta N_k^* \end{Bmatrix} \tag{7}$$

and where the symbol $\mathbf{J}^{-1}$ denotes the inverse of the well-known Jacobian matrix which coefficients can be easily calculated:

$$\mathbf{J} = \begin{bmatrix} \partial_\xi x & \partial_\xi y \\ \partial_\eta x & \partial_\eta y \end{bmatrix} = \sum_{k=1}^{36} \begin{bmatrix} \partial_\xi N_k^* x_k & \partial_\xi N_k^* y_k \\ \partial_\eta N_k^* x_k & \partial_\eta N_k^* y_k \end{bmatrix}. \tag{8}$$

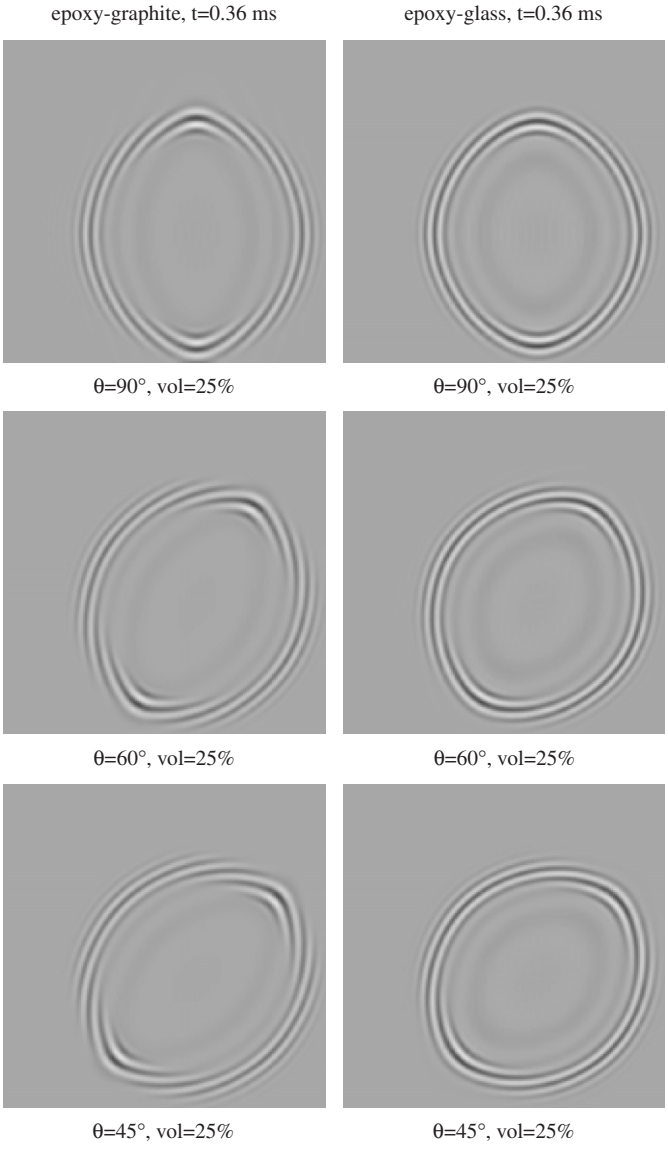

Fig. 8. Front of propagating transverse wave for a single layer.

The calculation of the characteristic mass **M** and stiffness **K** matrices of the spectral plate finite element follows the standard FE formulae and can be written in the following form:

$$\mathbf{M} = \rho \int_{-1}^{+1} \int_{-1}^{+1} \mathbf{N}^{\mathrm{T}}\mathbf{N} \det[\mathbf{J}]\, \mathrm{d}\eta\, \mathrm{d}\xi = \rho \sum_{m=1}^{6} \sum_{n=1}^{6} w_m w_n [N_{mn}]^{\mathrm{T}} [N_{mn}] \det[J_{mn}], \tag{9}$$

$$\mathbf{K} = \int_{-1}^{+1} \int_{-1}^{+1} \mathbf{B}^{\mathrm{T}}\mathbf{D}\mathbf{B} \det[\mathbf{J}]\, \mathrm{d}\eta\, \mathrm{d}\xi = \rho \sum_{m=1}^{6} \sum_{n=1}^{6} w_m w_n [B_{mn}]^{\mathrm{T}} \mathbf{D} [B_{mn}] \det[J_{mn}], \tag{10}$$

where **D** denotes the matrix of elastic coefficients for composite materials (see Appendix A) while w_m and w_n are the Gauss–Lobatto weights calculated at the element nodes m and n from the following formula [43]

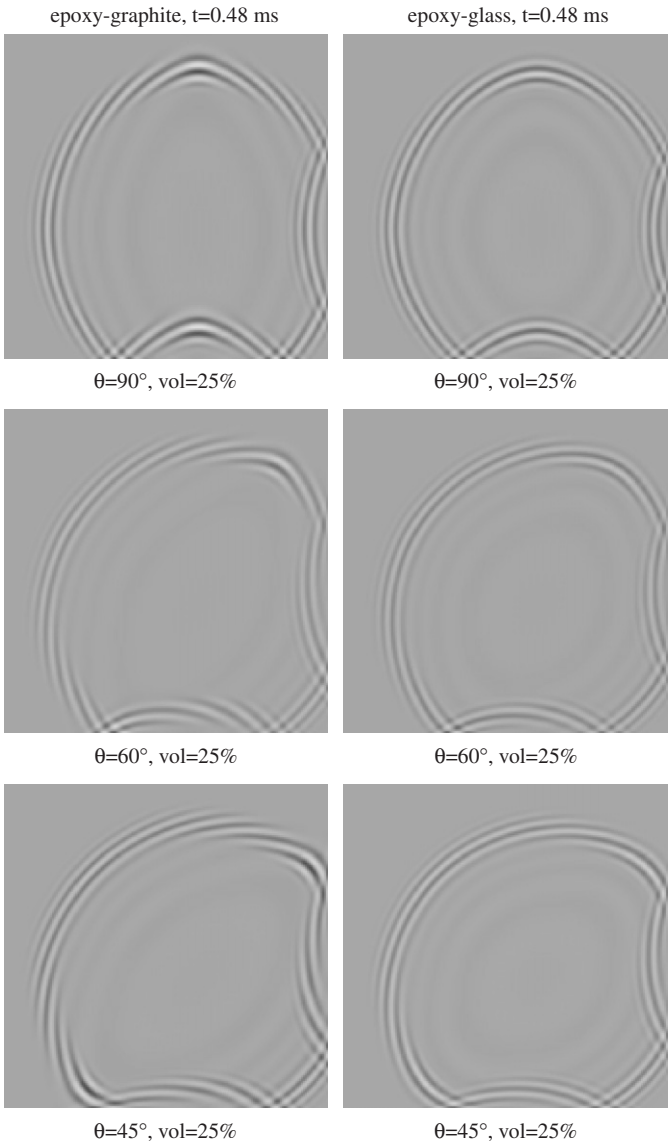

Fig. 9. Front of propagating transverse wave for a single layer.

(see also Eq. (2)):

$$w_{m,n} = \frac{1}{15P_5(\xi_{m,n})}, \quad m,n = 1,\ldots,6. \tag{11}$$

Due to the fact that the element approximation shape functions are orthogonal, as shown by Eq. (4), the element mass matrix **M** is diagonal.

In the presence of no damping the equation of motion can be easily discretised and solved in the time domain by applying the central difference time integration scheme:

$$\mathbf{M}\ddot{\mathbf{q}}_t + \mathbf{K}\mathbf{q}_t = \mathbf{Q}(t)_t - \mathbf{F}_t, \tag{12}$$

where the symbol t denotes time, $\mathbf{Q}(t)$ is the vector of excitation forces, and **F** is the vector of internal forces. The symbols **q** and $\ddot{\mathbf{q}}$ denote here the vectors of nodal displacement and nodal accelerations.

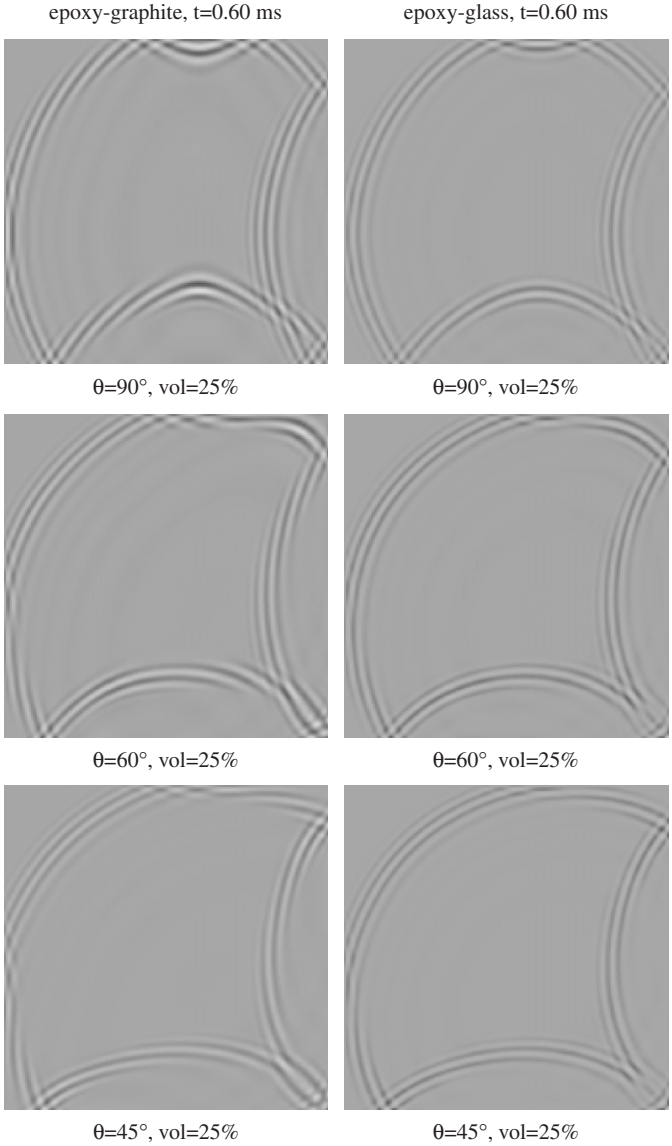

Fig. 10. Front of propagating transverse wave for a single layer.

Because of the diagonal form of the global mass matrix **M** the equation of motion can be further simplified and written as [44]

$$\mathbf{q}_{\alpha_{t+\Delta t}} = \frac{\mathbf{R}_{\alpha_t}}{P_{\alpha\alpha}},$$
$$\mathbf{R}_{\alpha_t} = \mathbf{Q}_{\alpha_t} - \mathbf{F}_{\alpha_t} - \left[\mathbf{K} - \frac{2}{\Delta t^2}\mathbf{M}\right]_{\alpha\alpha}\mathbf{q}_{\alpha_t} - \frac{1}{\Delta t^2}\mathbf{M}_{\alpha\alpha}\mathbf{q}_{\alpha_{t-\Delta t}},$$
$$\mathbf{P}_{\alpha\alpha} = \frac{1}{\Delta t^2}\mathbf{M}_{\alpha\alpha}, \tag{13}$$

where the symbol α denotes the successive global dof and Δt is a time increment. The solution of the equation of motion, based on such a procedure, is very fast and effective due to the diagonal form of the mass matrix.

3. Numerical calculations

3.1. Geometry definition and material properties

The geometry of a composite plate under investigation is presented in Fig. 4. The length and the width of the plate is 1000 mm. It is assumed that the plate is made out of glass-epoxy or graphite-epoxy composite material.

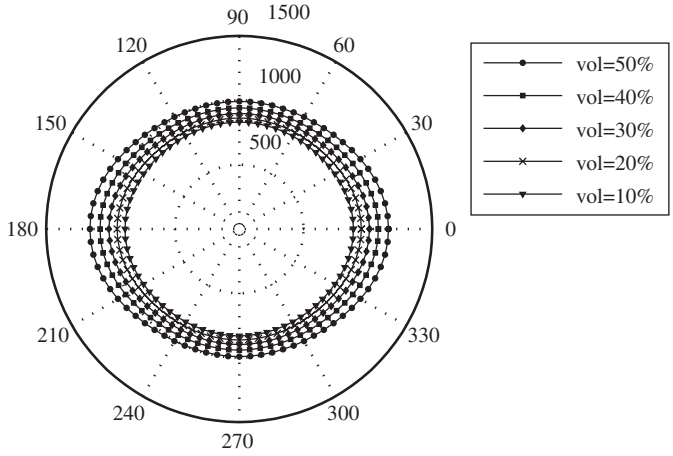

Fig. 11. Group velocity surfaces for a single layer of glass/epoxy laminates ($\theta = 0^\circ$, vol = 10%, 20%, 30%, 40% and 50%, $V_{max} = 0.951$, 1.022, 1.090, 1.162, 1.238 [km/s]).

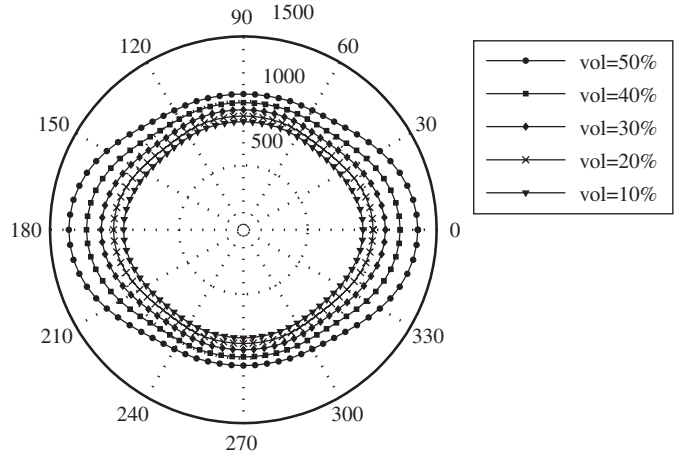

Fig. 12. Group velocity surfaces for a single layer of graphite/epoxy laminates ($\theta = 0^\circ$, vol = 10%, 20%, 30%, 40% and 50%, $V_{max} = 1.028$, 1.122, 1.227, 1.348, 1.489 [km/s]).

The following material data have been used: for the reinforcing glass fibres: Young's modulus $E = 66.5\,\text{GPa}$, Poisson ratio $v = 0.23$, and density $\rho = 2250\,\text{kg/m}^3$, for the reinforcing graphite fibres: Young's modulus $E = 275.6\,\text{GPa}$, Poisson ratio $v = 0.20$, and density $\rho = 1900\,\text{kg/m}^3$, whereas for the epoxy matrix Young's modulus $E = 3.43\,\text{GPa}$, Poisson ratio $v = 0.35$, and density $\rho = 1250\,\text{kg/m}^3$. The orientation angle θ of the reinforcing fibres and their relative volume fraction *vol* have been assumed as variable in the present analysis.

First, a single layer composite plate 10 mm thick is investigated. Next a multilayer composite plate consisting of 10 layers of composite material, each layer 1 mm thick, is analysed.

In all numerical examples the same mesh of 40×40 spectral plate elements has been used which results in 121,203 dof. The time of the analysis has been assumed as equal to 0.0012 s divided by 5000 time integration steps.

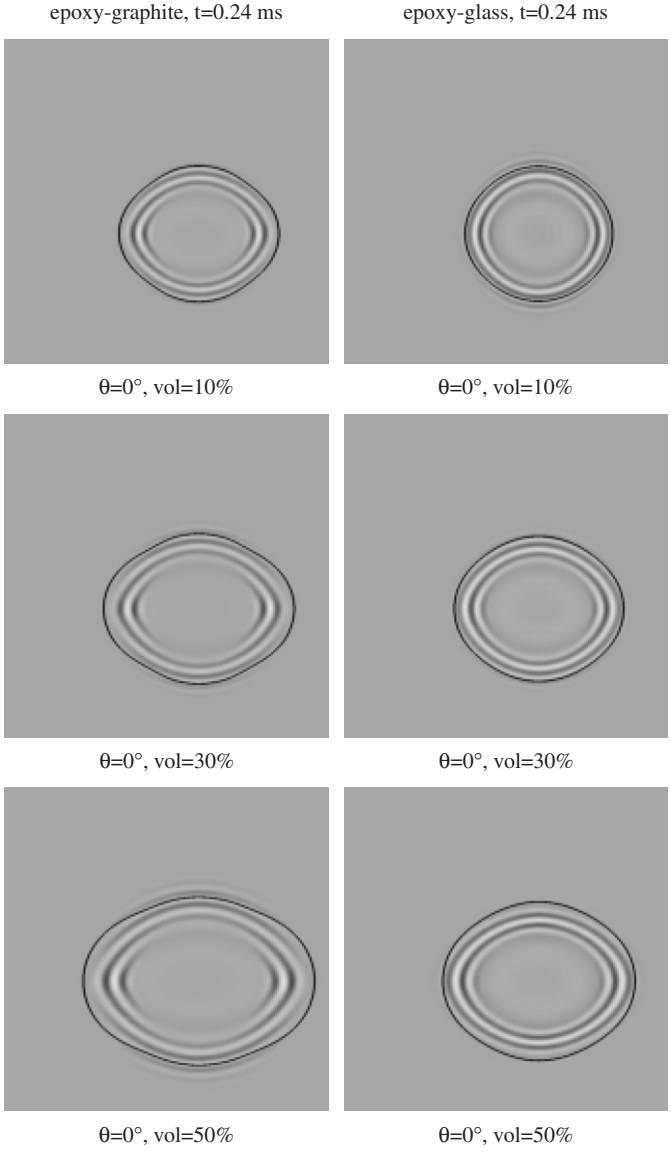

Fig. 13. Front of propagating transverse wave for a single layer.

3.2. Influence of the orientation of reinforcing fibres on wave propagation

In this section numerical calculations have been carried out for a single layer composite plate presented in Fig. 4 with free boundary conditions (all four edges of the plate free). In all cases considered here the relative volume fraction of the fibres is equal to 0.25. An excitation signal in the form of a force pulse signal of 100 N amplitude has been applied at point A, and is presented in Fig. 5 in both time and frequency domains. The frequency of the carrier signal is 25 kHz with three cycles, which is below the so-called 'cut-off' frequency, also marked in Fig. 5. The 'cut-off' frequency is calculated for the single layer of the glass-epoxy laminate (compare with Fig. 14). This means that only the A0 Lamb wave mode should be observed during the analysis. The influence of the fibre orientation on the propagation of the transverse elastic waves in the plate has been investigated.

For the current case the group velocity c_g of the transverse wave is not constant, but is a function of the relative volume fraction of the fibres, the direction of propagation and also depends on the frequency of the signal. This velocity can be calculated analytically by a procedure shown in Appendix A. The velocities calculated theoretically enable one verification of the correctness of the results of numerical simulation.

For the single layer composite plate analysed wave propagation velocities related to the local direction parallel to the reinforcing fibres x' and the local direction perpendicular to the fibres y' have the following values:

For glass-epoxy material:

$$c_{gx'} = 1056.35 \text{ m/s}, \quad c_{gy'} = 916.03 \text{ m/s}.$$

For graphite-epoxy material:

$$c_{gx'} = 1172.82 \text{ m/s}, \quad c_{gy'} = 941.80 \text{ m/s}.$$

Using the values of the velocities calculated in Eq. (A.6) it is very easy to estimate the time t needed for a propagating elastic wave to travel from the excitation point A to points B, C or D (Fig. 4). Taking into account the geometry of the plate as well as the wave propagation velocities the time t can be easily calculated for each case.

The group velocity depends on the direction of wave propagation, so the group velocity surface can be plotted in a polar coordinate as presented in Fig. 6. It is shown that the front of the propagating wave is retained, while elliptic-like elongation rotates according to the orientation angle of the fibres θ.

Certain results on the influence of the orientation of the reinforcing graphite and glass fibres on the shapes of propagating transverse waves are shown in Figs. 7–10. It is clearly visible that the orientation of the fibres is the main factor influencing the propagating waves.

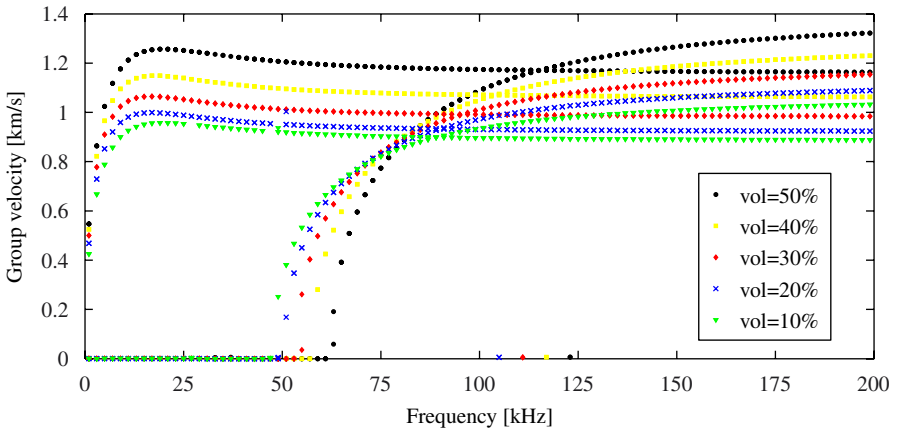

Fig. 14. Group wave speed as a function of the frequency (single layer of glass/epoxy laminate, vol = 10%, 20%, 30%, 40% and 50%).

3.3. Influence of the relative volume fraction of reinforcing fibres on wave propagation

The relative volume fraction is a factor which influences the velocity of propagating waves. An increase in the relative volume fraction of the reinforcement in a composite material results in an increase in the velocity of propagating waves as shown in Figs. 11 and 12. It should be noticed that the group velocities for the glass-epoxy layer (Fig. 11) substantially differ from the graphite-epoxy velocities (Fig. 12). In the second case, the shapes of the group wave surfaces are also sharper.

It can be expected that the shape of propagating waves is similar to those depicted in previous figures. However, no monochromatic wave packets are considered. For this reason many wave components participate in the global motion influencing each other. Also imaginary parts of the roots of Eq. (A.5) indicate that evanescent waves are also present. As a result of that the patterns presented in Fig. 13 are obtained and wave fronts differ slightly from the velocity wave surfaces. The envelope presented in Fig. 13 show

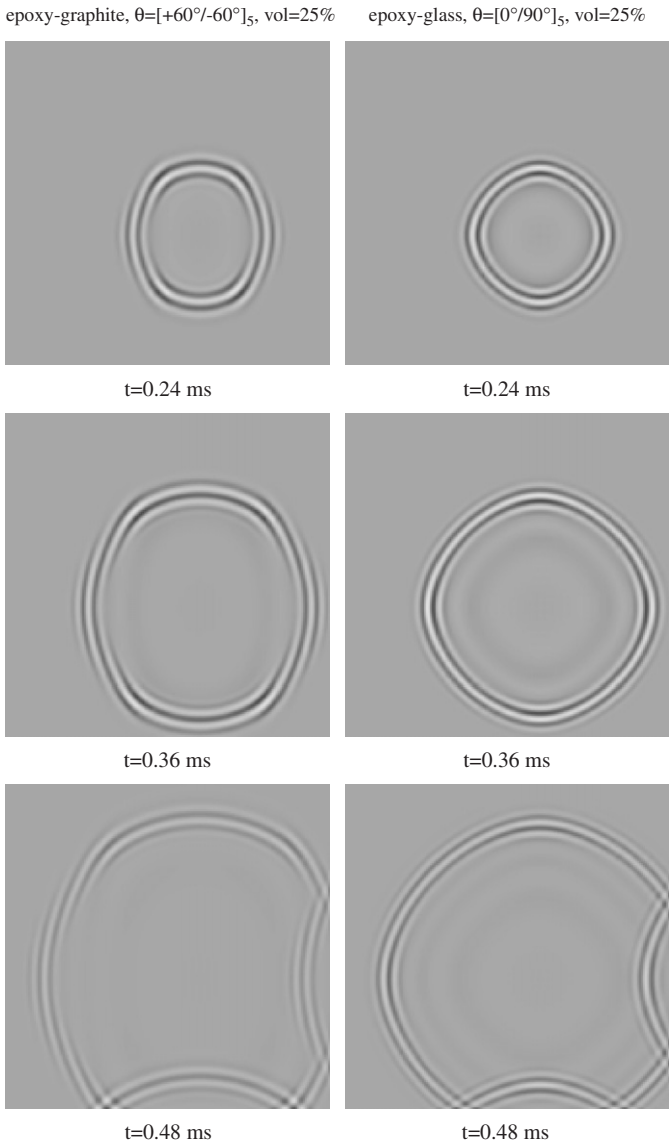

Fig. 15. Front of propagating transverse wave for a multilayer composite plate.

the theoretically calculated group velocity multiplied by an adequate time of analysis (as presented in Appendix A).

Fig. 14 shows the dependence of the group velocity on the frequency for the volume fractions of the reinforcement equal to: 10%, 20%, 30%, 40% and 50%. As the frequency increases the velocity increases as well. This relation is known as a dispersion curve. Dispersion relations are very important and cause additional problems in building appropriate damage detection algorithms. In Fig. 14, the second mode can be also observed propagating above cut-off frequency (around 50 kHz).

3.4. Wave propagation in a multilayer plate

In this case numerical calculations have been carried out for a 10 layer composite plate of the same geometry, boundary conditions, and the excitation signal as considered before. The assumed material for a single layer are glass-epoxy and graphite epoxy as in the previous example. The influence of the fibre

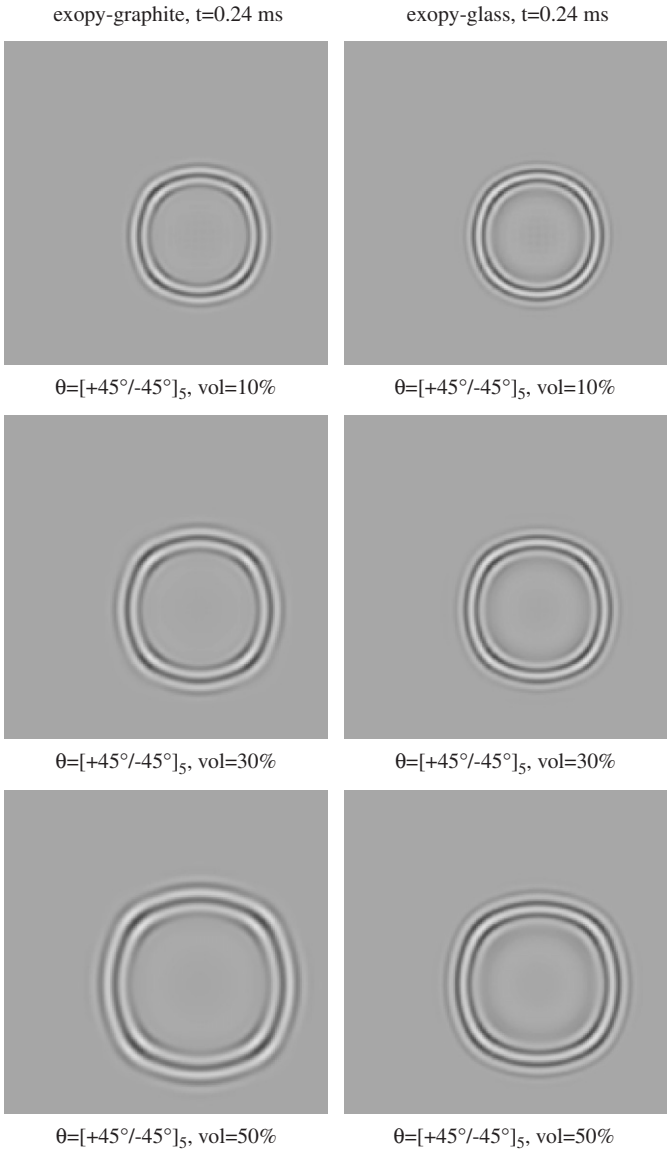

Fig. 16. Front of propagating transverse wave for a multilayer composite plate.

orientation has been investigated on the propagation of transverse waves in the plate. In this case the behaviour of propagating waves is more complicated than the behaviour observed in the case of the single layer composite plate. It is assumed that the shape of each travelling wave is a superposition of the waves travelling in each individual layer of the composite due to homogenization—see Fig. 15. It is also shown that the velocity of the propagating transverse elastic waves is a function of the volume fraction of the reinforcing fibres (a fact that has already been confirmed theoretically by Eq. (A.6)—see Fig. 16.

4. Conclusions

In this paper a spectral plate finite element has been successfully developed and applied for the analysis of elastic wave propagation in a composite plate for various orientations and relative volume fractions of reinforcing fibres. However, it has been noticed that certain instabilities of time integration schemes used for solving the equation of motion may arise. In order to overcome these problems a spatial sampling of the order of 4 to 5 points per minimum wavelength must be used and the time step should fulfils the Courant condition.

Results of numerical calculations indicate that the velocities of flexural waves travelling in composite materials are functions of the relative volume fraction of reinforcing fibres as well as the direction of propagation. Simple formulas for the calculation of the velocities of the flexural waves in composite materials have been presented and compared with the results of numerical calculations. These results show how the orientation of the fibres and the total number of layers influence the behaviour of propagating waves. This knowledge is an important factor from a practical point of view, especially for the design of appropriate monitoring systems utilising anomalies in the propagation of elastic waves.

In the opinion of the authors the SEM approach presented can easily be modified and adopted for use in the case of 3D structural elements or structural elements with damage in the form of cracks, delamination, etc.

Acknowledgements

The authors gratefully acknowledge the support for this research provided by the EU under the Sixth EU Framework Programme for Research and Technological Development (FP6) via ARTIMA project (Aircraft Reliability Through Intelligent Materials Application—reference number 502725), and also wish to thank the Polish Ministry of Education and Science.

Appendix A

The strain–stress matrix $\mathbf{D}$ in the case of composite material may be expressed in the following way:

$$\mathbf{D} = \begin{bmatrix} D_{11} & D_{12} & D_{16} & 0 & 0 \\ D_{12} & D_{22} & D_{26} & 0 & 0 \\ D_{16} & D_{26} & D_{66} & 0 & 0 \\ 0 & 0 & 0 & A_{44} & A_{45} \\ 0 & 0 & 0 & A_{45} & A_{55} \end{bmatrix}, \tag{A.1}$$

where the elements of the matrix $\mathbf{D}$ can be calculated as defined in Ref. [1].

The group velocities can be calculated by means of the following procedure. Assuming wave propagation solutions in the following form:

$$\begin{aligned} w(x,y,t) &= w_0 \exp(-\mathrm{i}kx\cos\theta)\exp(-\mathrm{i}ky\sin\theta)\exp(-\mathrm{i}\omega t), \\ \alpha(x,y,t) &= \alpha_0 \exp(-\mathrm{i}kx\cos\theta)\exp(-\mathrm{i}ky\sin\theta)\exp(-\mathrm{i}\omega t), \\ \beta(x,y,t) &= \beta_0 \exp(-\mathrm{i}kx\cos\theta)\exp(-\mathrm{i}ky\sin\theta)\exp(-\mathrm{i}\omega t), \end{aligned} \tag{A.2}$$

where w_0, α_0, β_0 are wave amplitudes and θ denotes the angle between the global and the local material axes. Substitution of these solutions into the Mindlin's equations of motion [2] results in the set of equations which

can be written as

$$\begin{bmatrix} H_{11}(k) & H_{12}(\omega,k) & H_{13}(k) \\ H_{21}(k) & H_{22}(k) & H_{23}(\omega,k) \\ H_{31}(k) & H_{32}(k) & H_{33}(k) \end{bmatrix} \begin{Bmatrix} w_0 \\ \alpha_0 \\ \beta_0 \end{Bmatrix} = \begin{Bmatrix} 0 \\ 0 \\ 0 \end{Bmatrix}, \tag{A.3}$$

where the elements of the matrix **H** are:

$$\begin{cases} H_{11} = \mathrm{i}kmA_{44} + \mathrm{i}knA_{45}, \\ H_{12} = I\omega^2 - A_{44} - k^2m^2D_{11} - 2k^2mnD_{16} - k^2n^2D_{66}, \\ H_{13} = -A_{45} - k^2mnD_{12} - k^2m^2D_{16} - k^2n^2D_{26} - k^2mnD_{66}, \\ H_{21} = \mathrm{i}kmA_{45} + \mathrm{i}knA_{55}, \\ H_{21} = H_{13}, \\ H_{23} = I\omega^2 - A_{55} - k^2n^2D_{22} - 2k^2m^2nD_{26} - k^2m^2D_{66}, \\ H_{31} = h\rho\omega^2, \\ H_{32} = \mathrm{i}k^3m^3D_{11} + \mathrm{i}k^3mn^2D_{12} + 3\mathrm{i}k^3m^2nD_{16} + \mathrm{i}k^3n^3D_{26} + 2\mathrm{i}k^3mn^2D_{66}, \\ H_{33} = \mathrm{i}k^3m^2nD_{12} + \mathrm{i}k^3m^3D_{16} + \mathrm{i}k^3n^3D_{22} + 3\mathrm{i}k^3mn^2D_{26} + 2\mathrm{i}k^3m^2nD_{66}, \end{cases} \tag{A.4}$$

and where $\mathrm{i} = \sqrt{-1}$, the mass inertia $I = \frac{1}{3}\sum_{k=1}^{N}\rho[h_k^3 - h_{k-1}^3]$, $\omega = 2\pi f$.

The next calculation of the determinant of the matrix **H** leads to the following relation:

$$a_6k^6 + a_4k^4 + a_2k^2 + a_0 = 0, \quad a_i = a_i(\omega), \quad i = 0, 2, 4, 6. \tag{A.5}$$

There are six roots of this equation which correspond to three sets of mode pairs. The group velocities of the first real propagating mode can be calculated numerically from:

$$c_g = \frac{\mathrm{d}\omega}{\mathrm{d}k_1}. \tag{A.6}$$

References

[1] J.R. Vinson, R.L. Sierakowski, *Behavior of Structures Composed of Composite Materials*, Martinus-Nijhoff, Inc., 1989.
[2] O.O. Ochoa, J.N. Reddy, *Finite Element Analysis of Composite Laminates*, Kluwer Academic Publishers, Dordrecht, 1992.
[3] J.M. Whitney, *Structural Analysis of Laminated Anisotropic Plates*, Technomic Publishing Co., 1987.
[4] A.L. Kalamkarov, *Composite and Reinforced Elements of Construction*, Wiley, New York, 1992.
[5] R.M. Jones, *Mechanics of Composite Materials*, Taylor & Francis Inc., London, 1999.
[6] M. Krawczuk, W.M. Ostachowicz, A. Żak, Dynamics of cracked composite structures, *Computational Mechanics* 20 (1997) 79–83.
[7] L.J. Bond, Numerical techniques and their use to study wave propagation and scattering: a review, in: S.K. Datta, J.D. Achenbach, Y.S. Rajapakse (Eds.), *Elastic Waves and Ultrasonic Non-destructive Evaluation*, North-Holland, Amsterdam, 1990.
[8] J.C. Strickwerda, *Finite Difference Schemes and Partial Differential Equations*, Wadsworth-Brooks, Belmont, 1989.
[9] H. Yamawaki, T. Saito, Numerical calculation of surface waves using new nodal equation, *NDT&E International* 8–9 (1992) 379–389.
[10] O.C. Zienkiewicz, *The Finite Element Method*, McGraw-Hill, New York, 1989.
[11] R.J. Talbot, J.S. Przemieniecki, Finite element analysis of frequency spectra for elastic waves guides, *International Journal of Solids and Structures* 11 (1976) 115–138.
[12] M. Koshiba, S. Karakida, M. Suzuki, Finite element analysis of Lamb waves scattering in an elastic plate waveguide, *IEEE Transactions on Sonic and Ultrasonic* 31 (1984) 18–25.
[13] G.S. Verdict, P.H. Gien, C.P. Burger, Finite element study of Lamb wave interactions with holes and through thickness defects in thin metal plates, in: D.O. Thompson, D.E. Chimenti (Eds.), *Review of Progress in Quantitative Non-destructive Evaluation*, Vol. 11, 1992, pp. 97–104.
[14] D.N. Alleyne, P. Cawley, Optimization of lamb wave inspection techniques, *NDT&E International* 25 (1992) 11–22.
[15] C.A. Brebbia, J.C.F. Tells, L.C. Wrobel, *Boundary Elements Techniques*, Springer, Berlin, 1984.
[16] Y. Cho, J.L. Rose, A boundary element solution for mode conversion study of the edge reflection of Lamb waves, *Journal of the Acoustical Society of America* 99 (1996) 2079–2109.
[17] Y.K. Cheung, *Finite Strip Method in Structural Analysis*, Pergamon Press, Oxford, 1976.
[18] G.R. Liu, Z.C. Xi, *Elastic Waves in Anisotropic Laminates*, CRC Press, Boca Raton, 2002.
[19] G.R. Liu, J. Tani, K. Watanabe, T. Ohyoshi, Harmonic wave propagation in anisotropic laminated strips, *Journal of Sound and Vibration* 139 (1990) 313–330.

[20] T. Liu, K. Liu, J. Zhang, Unstructured grid method for stress wave propagation in elastic media, *Computer Methods in Applied Mechanics and Engineering* 193 (2004) 2427–2452.
[21] T. Liu, K. Liu, J. Zhang, Triangular grid method for stress-wave propagation in 2-D orthotropic materials, *Archive of Applied Mechanics* 74 (2005) 477–488.
[22] P.P. Delsanto, R.B. Mignogna, A spring model for the simulation of the ultrasonic pulses through imperfect contact interfaces, *Journal of Acoustical Society of America* 104 (1998) 1–8.
[23] H. Yim, Y. Sohn, Numerical simulation and visualization of elastic waves using mass-spring lattice model, *IEEE Transactions on Ultrasonic, Ferroelectrics, and Frequency Control* 47 (2000) 549–558.
[24] P.P. Delsanto, T. Whitecomb, H.H. Chaskelis, R.B. Mignogna, Connection machine simulation of ultrasonic wave propagation in materials. I: the one-dimensional case, *Wave Motion* 16 (1992) 65–80.
[25] P.P. Delsanto, T. Whitecomb, H.H. Chaskelis, R.B. Mignogna, R.B. Kline, Connection machine simulation of ultrasonic wave propagation in materials. II: the two-dimensional case, *Wave Motion* 20 (1994) 295–314.
[26] P.P. Delsanto, R.S. Schechter, R.B. Mignogna, Connection machine simulation of ultrasonic wave propagation in materials. III: the three-dimensional case, *Wave Motion* 26 (1997) 329–339.
[27] J.F. Doyle, *Wave Propagation in Structures*, Springer, Berlin, 1997.
[28] A.T. Patera, A spectral element method for fluid dynamics : laminar flow in a channel expansion, *Journal of Computational Physics* 54 (1984) 468–488.
[29] M. Krawczuk, M. Palacz, W. Ostachowicz, The dynamic analysis of cracked Timoshenko beam by the spectral element method, *Journal of Sound and Vibration* 264 (2003) 1139–1153.
[30] D.R. Mahapatra, S. Golpalakrishnan, A spectral finite element model for analysis of axial–flexural–shear coupled wave propagation in laminated composite beams, *Computers and Structures* 59 (2003) 67–88.
[31] M. Palacz, M. Krawczuk, Analysis of longitudinal wave propagation in a cracked rod by the spectral element method, *Computers and Structures* 80 (2002) 1809–1816.
[32] A. Chakraborty, S. Gopalakrishnan, A spectrally formulated plate element for wave propagation analysis in anisotropic material, *Computer Methods in Applied Mechanics and Engineering* 194 (2005) 4425–4446.
[33] A. Chakraborty, S. Gopalakrishnan, An approximate spectral element for the analysis of wave propagation in inhomogeneous layered media, *AIAA Journal* 44 (2006) 1676–1685.
[34] A. Chakraborty, S. Gopalakrishnan, A spectral finite element model for wave propagation analysis in laminated composite plate, *ASME Journal of Vibration and Acoustics* 128 (2006) 477–488.
[35] J.P. Boyd, *Cheybyshev and Fourier spectral methods*, Springer, Berlin, 1989.
[36] C. Pozrikidis, *Introduction to Finite and Spectral Element Methods using MATLAB®*, Chapman & Hall/CRC, London/Boca Raton, 2005.
[37] C. Canuto, M.Y. Hussaini, A. Quarteroni, T.A. Zang, *Spectral Methods in Fluid Dynamics*, Springer, Berlin, 1988.
[38] R. Spall, Spectral collocation methods for one dimensional phase change problems, *International Journal of Heat and Mass Transfer* 15 (1995) 2743–2748.
[39] W. Dauksher, A.F. Emery, The use of spectral methods in predicting the reflection and transmission of ultrasonic signals through flaws, in: D.O. Thompson, D.E. Chimenti (Eds.), *Review of Progress in Quantitative Non-destructive Evaluation*, Vol. 15, 1996, pp. 97–104.
[40] G. Seriani, 3-D large scale wave propagation modelling by spectral element method on Cray T3E multiprocessor, *Computational Methods Applied in Mechanical Engineering* 164 (1998) 235–247.
[41] D. Komatitsch, Ch. Barnes, J. Tromp, Simulation of anisotropic wave propagation based upon a spectral element method, *Geophysics* 65 (2000) 1251–1260.
[42] R. Sridhar, A. Chakraborty, S. Gopalakrishnan, Wave propagation in a anisotropic and inhomogeneous uncracked and cracked structures using pseudospectral finite element method, *International Journal of Solids and Structures* 43 (2006) 4997–5031.
[43] http://mathworld.wolfram.com.
[44] M. Kleiber, *Incremental Finite Element Modelling in Non-linear Solid Mechanics*, Wiley, New York, 1989.